ARCHIVOS DE LA SOCIEDAD ESPAÑOLA DE OFTALMOLOGÍA

www.elsevier.es/oftalmologia

Original article

# Automated detection of microaneurysms by using region growing and fuzzy artmap neural network☆,☆☆

S. Jiménez[a,b,*], P. Alemany[a,b], F.J. Núñez[c], I. Fondón[c], C. Serrano[c], B. Acha[c], I. Failde[d]

[a] Servicio de Oftalmología, Hospital Universitario Puerta del Mar, Cádiz, Spain
[b] Departamento de Cirugía, Facultad de Medicina, Universidad de Cádiz, Cádiz, Spain
[c] Departamento de Teoría de la Señal y Comunicaciones, Escuela Técnica Superior de Ingeniería, Universidad de Sevilla, Sevilla, Spain
[d] Departamento de Biomedicina, Biotecnología y Salud Pública, Facultad de Medicina de Fisioterapia, Universidad de Cádiz, Cádiz, Spain

ARTICLE INFO

*Article history:*
Received 28 January 2012
Accepted 8 April 2012
Available online 24 October 2012

*Keywords:*
Computer aided diagnosis
Fundus photography
Diabetic retinopathy screening
Microaneurysm
Neural network

ABSTRACT

*Objective:* To assess whether the methodological changes of this new algorithm improves the results of a previously presented strategy.
*Methods:* We enhance the image and filter out the green channel of the digital color retinography. Multitolerance thresholding was applied to obtain candidate points and make a seed growing region by varying intensities. We took 15 characteristics from each region to train a fuzzy Artmap neural network using 42 retinal photographs. This network was then applied in the study of 11 good quality retinal photographs included in the diabetic retinopathy early detection screening program, with initial stages of retinopathy, obtained with the Topcon NW200 non-mydriatic retinal camera.
*Results:* Two experienced ophthalmologists detected 52 microaneurysms in 11 images. The algorithm detected 39 microaneurysms and 3752 more regions, confirming 38 microaneurysm and 135 false positives. The sensitivity is improved compared to the previous algorithm, from 60.53% to 73.08%. False positives have dropped from 41.8 to 12.27 per image.
*Conclusions:* The new algorithm is better than the previous one, but there is still room for improvement, especially in the initial determination of seeds.

© 2012 Sociedad Española de Oftalmología. Published by Elsevier España, S.L. All rights reserved.

## Detección automatizada de microaneurismas mediante crecimiento de regiones y red neuronal Fuzzy Artmap

*Palabras clave:*
Diagnóstico asistido por ordenador
Retinografía
Detección de retinopatía diabética

RESUMEN

*Objetivo:* Comprobar si las modificaciones metodológicas de este nuevo algoritmo mejoran el resultado de otra estrategia presentada anteriormente.
*Métodos:* Se realza y filtra la imagen negada del canal verde de la retinografía digital en color. Se aplica una umbralización multitolerancia para obtener puntos candidatos

☆ Please cite this article as: Jiménez S, et al. Detección automatizada de microaneurismas mediante crecimiento de regiones y red neuronal Fuzzy Artmap. Arch Soc Esp Oftalmol. 2012;87:284–9.
☆☆ This paper was presented at the research session of the 86 SEO Congress held in Madrid on September 22, 2010.

* *Corresponding author.*
E-mail address: soledadjimenez@ono.com (S. Jiménez).

2173-5794/$ – see front matter © 2012 Sociedad Española de Oftalmología. Published by Elsevier España, S.L. All rights reserved.

Microaneurismas
Red neuronal

y en cada semilla se realiza un crecimiento de regiones por variación de intensidades. Se toman 15 características de cada región y entrenamos una red neuronal Fuzzy Artmap con 42 retinografías. Se aplica la red en el estudio de 11 retinografías del programa de detección precoz de retinopatía diabética, de buena calidad, con lesiones iniciales, obtenidas con el retinógrafo no midriático Topcon NW200.

*Resultados:* Dos oftalmólogos experimentados detectan 52 microaneurismas en las 11 imágenes. El algoritmo detecta 39 microaneurismas y 3.752 regiones más, confirmando 38 microaneurismas y 135 falsos positivos. La sensibilidad ha mejorado respecto al algoritmo anterior del 60,53 al 73,08%. Los falsos positivos has disminuido de 41,8 por imagen a 12,27.

*Conclusiones:* El nuevo algoritmo presenta indudables mejoras respecto al anterior, pero aún se puede perfeccionar, sobre todo en la determinación inicial de semillas.

© 2012 Sociedad Española de Oftalmología. Publicado por Elsevier España, S.L. Todos los derechos reservados.

## Introduction

Diabetic retinopathy is the most frequent cause of new adult blindness cases for age groups between 20 and 74 years.[1] Diabetic retinopathy detection programs focus on identifying injuries that point to the disease (among others, microaneurysms) in color digital photographs taken with non-midriatic retinographs in the target population.[2] The size and color of microaneurysms make them easily identifiable by primary care physicians involved in detection programs. In addition, the localization process is tedious and slow, even for specialists. For these reasons it is necessary to devise an automated system to quickly and efficiently detect microaneurysms. To this end, algorithms were developed to enhance microaneurysms candidate injuries, eliminate other ocular fundus elements and establish different characteristics to classify candidates as true microaneurysms.[3–6] This paper presents an improved algorithm for detecting microaneurysms in color digital photographs of patients with diabetic retinopathy and the diagnostic usefulness thereof.

## Materials and methods

### *Algorithm development*

The method utilized in this paper is summarized in the schema illustrated in Fig. 1. During the preprocessing phase the green negated channel (*gneg*) is obtained from the RGB image. In this channel the shiny elements that represent the optic disk and exudates (if any) are segmented by histogram thresholding, obtaining a binary image where the pixels belonging to said elements have a value of 1 and the remainder will have a value of zero. Subsequently, the vascular tree is segmented with a multi-tolerance thresholding method[7] where a threshold condition depending on the surface occupied by the vascular tree is added. The result is a binary image where the pixels belonging to the vascular tree have a value of 1 and the rest of the image has a value of zero. Said binary image is combined with the shiny elements image to attain a binary mask ($m_{bin}$).

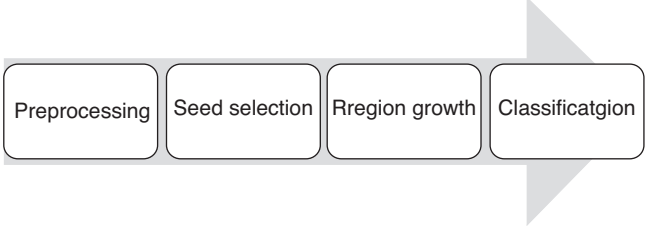


**Fig. 1 – Algorithm flow diagram.**

After the vascular tree segmentation, *gneg* is submitted to a polynomic contrast enhancing process which produces the *C*(*gneg*) image. Subsequently, the image is submitted to 2 successive filterings. Firstly, a $3 \times 3$ pixel Gaussian filter is applied having a value of $\sigma = 2$. Then this image is submitted to a high step filtering to remove the fundus and maintain the elements that constitute a sudden change in image intensity, thus obtaining the standardized image <*HP*(*C*(*gneg*))>. Finally, the vascular tree and the shiny elements detected in $m_{bin}$ are removed from the image, which causes that the remaining pixels have a value of zero. Fig. 2 illustrates the preprocessing schema and Fig. 3 shows an example with some of the images obtained with said preprocessing.

The next step consists of illuminating the vascular tree and shiny elements from the <*HP*(*C*(*gneg*))> image, so that all the pixels present in $m_{bin}$ are 0.

In the Seed Selection phase, a new multi-tolerance thresholding of the image is carried so render a maximum of 1000 regions which could be microaneurysm seeds. During thresholding, the pixel with highest intensity in each segmented region is marked as a seed candidate. These potential seeds are subsequently validated by calculating for each the statistical *tail ratio* that provides information about the distribution of intensities in the histogram of a window centered on the pixel being studied.[8]

In each selected seed a region growth is applied in which neighboring pixels are added having an intensity above the mean value plus the typical deviation of a window centered on the seed having a size of $10 \times 10$ pixels. For the growing region to be valid it must not have a surface exceeding 30 pixels because in our database and at the resolution we work with there is no microaneurysm having an extension above said value (Fig. 4).

In order to classify regions, 15 characteristics are calculated for each grown seed—numbered from 1 to 15–of which 4 are

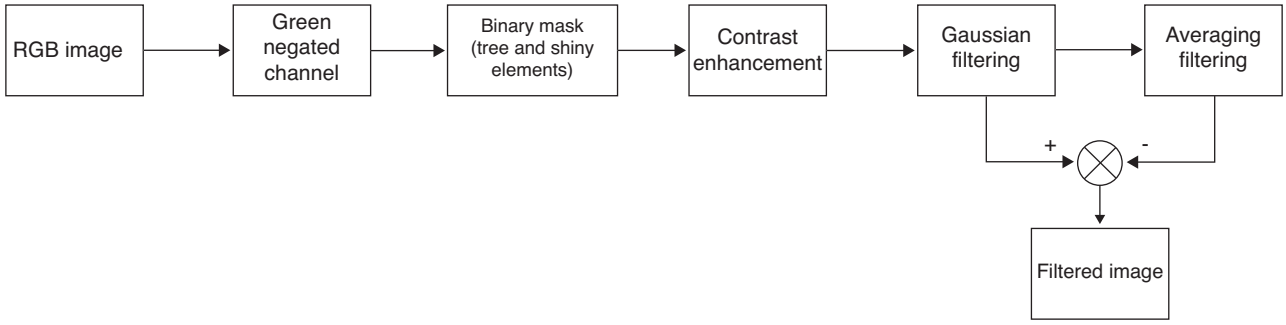


**Fig. 2 – Preprocessing schema.**

calculated on the basis of the binary representation of each grown region, 4 on the basis of the *gneg* image, 4 on the basis of the *C*(*gneg*) image and 3 on the basis of the <*HP*(*C*(*gneg*))> image. The binary image only counts with pixels having values of zero and one, without quantifiable intensity of contrast differences. It is the most adequate image to determine morphological parameters. The 4 characteristics are:

1) Surface ($S_i$): sum of pixels belonging to region i.
2) Aspect ratio: the result of dividing the larger diameter by the smaller diameter of the region.
3) Perimeter ($P_i$): the number of pixels located at the edge of region i.
4) Circularity ($C_i$): this characteristic provides information about the shape of region i, and is calculated by means of $C_i = P_i^2/(4\pi S_i)$.

The 4 characteristics taken on the basis of regions in *gneg* are:

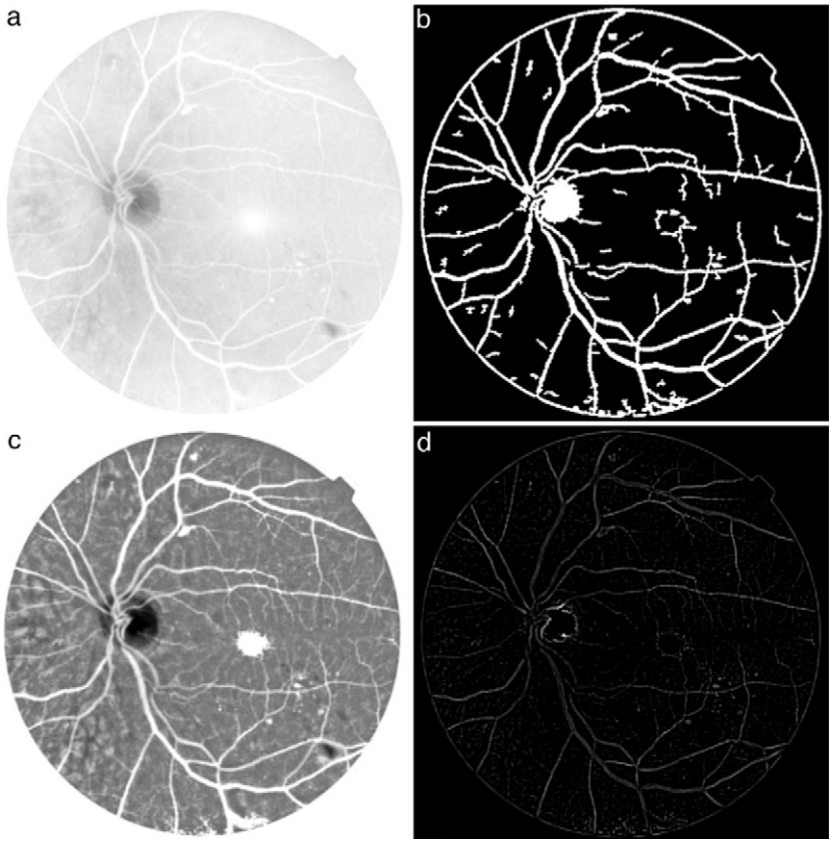


**Fig. 3 – (a) *gneg*, (b) $m_{bin}$, (c) *C*(*gneg*), and (d) <*HP*(*C*(*gneg*))>.**

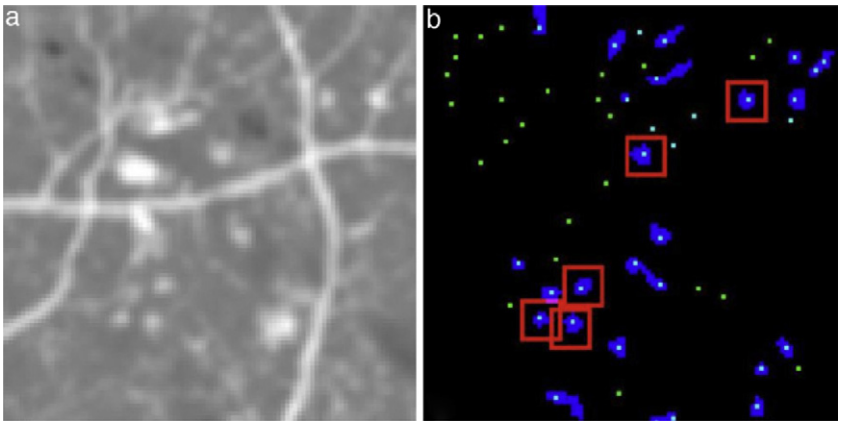


**Fig. 4 – (a) Cutout of *C(gneg)*. (b) Result of the region growth in the cutout: the lighter points of the seed pixels detected by the algorithm; the gray extensions are the candidate points with the final region growth. The microaneurysms detected by the specialist are shown within red squares.**

1) Mean intensity A (<IiA>): the sum of the pixel intensities of region i divided by the surface of said region.
2) Correlation with Gaussian A: provides information about the similarity of region i with a Gaussian structural element of the same size of region i.
3) Contrast A: it measures the difference between the mean intensity of region i pick cells and adjacent pixels.
4) Fundus A mean intensity (<IfA>): the mean of pixels belonging to a window having a size of 15 × 15 pixels centered on the initial seed of each region.

The characteristics calculated on the basis of *C(gneg)* are:

1) Mean intensity B (<IiB>).
2) Correlation with Gaussian B.
3) Contrast B.
4) Fundus B mean intensity (<IfB>).

In order to obtain the <*HP*(*C*(*gneg*))> image, a high filter was applied to eliminate the fundus. For this reason, this image does not allow an assessment of the mean fundus intensity. The determined characteristics in this image are:

1) Mean intensity C (<IiC>).
2) Correlation with Gaussian C.
3) Contrast C.

A selection was made to determine characteristics with greater discriminating potential by means of forwarded sequential selection and backward sick when she'll alimentation. For classification, a Fuzzy Artmap[9] type neuronal network was utilized, which was trained with a group of images to subsequently classify a different group.

### *Retinographs*

The baseline was a database comprising 42 retinographs of the A Diabetic Retinopathy Early Detection Plan, the initial assessment of which must be carried out by primary health care physicians (PHP) of the hospital area for training the neuronal network. Said images were reviewed by 2 of the authors (SJ and PA) who pointed out 204 microaneurysms. Subsequently, 11 successive images were taken of 11 patients from the same early detection program diagnosed with diabetic retinopathy by the PHP and reviewed by the authors for evaluating the algorithm. The images were taken with a Topcon NW-200 retinograph and stored in the JPG format.

### *Computer equipment*

The algorithm was developed with the MATLAB 7.6.0 (R2008a; MathWorks) mathematical software on an HP Compaq dc7600 Convertible computer with an Intel® Pentium® 4 processor running on a CPU of 3.20 GHz and with 0.99 GB of RAM memory.

### *Statistics*

The average sensitivity of the algorithm and the number of false positives for each image was calculated.

## Results

Initially, 42 images with 204 microaneurysms were selected. During the seed selection process, seeds were placed in 167 microaneurysms. After region growth, the algorithm segmented 50,184 regions, of which 153 were microaneurysms (75%), and the remaining 15,031 were false positives. These were the regions of which the 15 characteristics discussed above were calculated. During the neuronal network training the best results were obtained with characteristics number 4, 7, 9, 13 and 15, obtaining an average sensitivity of 92.85% on the classification group, with the classifier exhibiting a hit rate of 92.45%.

Once the network was trained, the group of 11 retinographs containing 52 diagnosed microaneurysms was classified.

After the seed selection process and regional growth, a total amount of 32 segmented microaneurysms were obtained in addition to 3752 segmented regions that were not microaneurysms. After classifying said regions, 38 segmented microaneurysms were obtained together with 135 false positives, which translates into a sensitivity of 73.08% and a mean value of 12.27 false positives per image.

## Discussion

In the past various methods have been proposed for automatically detecting microaneurysms.[10–12] However, said methods have always been assessed with proprietary image databases which were different for each author and had different technical characteristics and reference parameters. Niemeijer et al. carried out an online experience in which they made available to various research groups an images database taken with non-midriatics retinographs, stored in JPEG format in order to apply various algorithms and with results recorded in a homogeneous manner by means of FROC curves.[2] In said study, they differentiated 4 types of microaneurysms. On the basis of their size and visibility these are: minimum, medium and evident. According to location, microaneurysms close to vessels are considered in a specific manner. A specific assessment was made for each microaneurysm type and an overall assessment in which the detection of the 4 types was taken jointly. In the 5 detection methods, executed by 5 research groups that accepted the online challenge, a direct relationship was appreciated between the greater sensitivity of the algorithm and the increase in the number of false microaneurysms per image. When the algorithms analyzed the total amount of microaneurysms, over 10 false microaneurysms were detected by image to raise sensitivity values between 50% and 60%.

On the basis of the images supplied in this study, the method developed by our research group presented in the 2009 CASEIB[7] was applied, obtaining sensitivity results of 16.53% and an average of 41.8 false positives per image. This represents a significant improvement vis-à-vis the previous methods and validity similar to that presented in the various methods of the online challenge.

The identification of small second or third order arterioles and venules as isolated segments is the most usual source of false microaneurysms. For this reason, the correct segmentation of the vascular tree is one of the key steps in automatic detection algorithms. In turn, the segmentations depend on the notoriety of the structures after completing image preprocessing and initial processing.

The next step in our research will focus on increasing the systems sensitivity by means of analyzing new approaches in region segmentation because this is where sensitivity is reduced the most. Our research continues to diminish the rate of false positives per image, including new pre- and post-processing methods that are currently in experimentation.

## Conclusions

With the algorithm presented in this paper, significant improvements have been obtained in the automatic detection of initial diabetic retinopathy injuries, increasing the sensitivity of the previous algorithm for microaneurysms from 60.53% to 73.08%, and diminishing the number of false positives per image from 41.08 to 12.27. However, the method still requires additional improvements so that the design tool can be compared to human detection with sufficient reliability to become a useful tool in clinical diabetic retinopathy detection programs.

## Funding

Funded by the Health Research Fund of Research Projects FIS ETES-PI07/90379, ETES-PI07/90373.

## Conflict of interests

No conflict of interests has been declared by the authors.

## REFERENCES

1. Fong DS, Aiello L, Gardner TW, King GL, Blankenship G, Cavallerano JD. Diabetic retinopathy. Diabetes Care. 2003;26:99–102.
2. Niemeijer M, van Ginneken B, Cree MJ, Mizutani A, Quellec G, Sanchez CI, et al. Retinopathy online challenge: automatic detection of microaneurysms in digital color fundus photographs. IEEE Trans Med Imaging. 2010;29:185–95.
3. Spencer T, Phillips RP, Sharp PF, Forrester JV. Automated detection and quantification of microaneurysms in fluorescein angiograms. Graefes Arch Clin Exp Ophthalmol. 1992;230:36–41.
4. Cree MJ, Olson JA, McHardy KC, Sharp PF, Forrester JV. A fully automated comparative microaneurysm digital detection system. Eye. 1997;11:622–8.
5. Sánchez CI, Hornero R, Mayo A, García M. Mixture model-based clustering and logistic regression for automatic detection of microaneurysms in retinal images. In: Karssemeijer N, Giger L, editors. SPIE medical imaging 2009: computer-aided diagnosis. Proceedings of SPIE, vol. 7260. 2009. p. 72601M1–M7.
6. Zhang B, Wu X, You J, Li Q, Karray F. Hierarchical detection of red lesions in retinal images by multiscale correlation filtering. In: Karssemeijer N, Giger L, editors. SPIE medical imaging 2009: computer-aided diagnosis. Proceedings of SPIE, vol. 7260. 2009. p. 72601L1–L6.
7. Núñez FJ, Serrano C, Acha B, Fondón I, Jiménez S, Alemany P. Detección Automática de Microaneurismas en Retinografías para Diagnóstico Precoz de Retinopatía Diabética. CASEIB. 2009;27:581–4.
8. Acha B, Serrano C, Rangayyan RM. Detection of microcalcifications in mammograms using 2d prediction filtering and a new statistical measure of the right tail weight. Proc Embec. 2005:3112–7.
9. Carpenter A. Fuzzy ARTMAP: a neural network architecture for incremental supervised learning of analog multidimensional maps. IEEE Trans Neural Netw. 1992;3:698–713.

10. Niemeijer M, van Ginneken B, Staal J, Suttorp-Schulten MSA, Abramoff MD. Automatic detection of red lesions in digital color fundus photographs. IEEE Trans Med Imaging. 2005;24:584–92.
11. Sinthanayothin C, Boyce JF, Williamson TH, Cook HL, Mensah E, Lal S, et al. Automated detection of diabetic retinopathy on digital fundus images. Diabet Med. 2002;19: 105–12.
12. Quellec G, Lamard M, Josselin PM, Cazuguel G, Cochener B, Roux C. Optimal wavelet transform for the detection of microaneurysms in retina photographs. IEEE Trans Med Imaging. 2008;27:1230–41.